An optimal design of smart charging station for personal mobility devices using multi-level bidirectional DC-DC converter

Abstract

Shrewd charging stations are important for PMDs like electric bikes, e-bicycles, and other convenient electric vehicles. These devices require regular charging to maintain their battery life and ensure their efficient operation. A smart charging station provides safe, convenient, and efficient charging solution for these devices, which can be easily accessible for users. The smart charging station aims to overcome the limitations of existing charging systems for PMDs by providing a solution that can meet There are voltage requirements for the majority of e-mobility devices, but charging current ripple is low. To achieve this, we design a deep multi-graph neural network (DMGNN) enabled multi-level bidirectional DC-DC converter to interconnect DC micro-grid with DC fast charging stations which is the capability to address voltage unbalance issues and effectively control the bidirectional power flow.Moreover, it outperforms the existing multi-level converters with High efficiency and a wide range of charging voltages in the low output voltage region. Additionally, a modified Emperor Penguin Optimization (MEPO) algorithm is applied to the optimization problem in order to precisely identify a number of decision variables involved in the creation of the most effective charging stations.At last, to affirm the viability of the proposed charging framework, we led reproductions and trials, including the improvement of a model charging framework.

Keywords:smart charging station, personal mobility devices, DC-DC converter, multi-level converter

1. Introduction

Personal mobility devices (PMDs) are small, lightweight, and portable electric vehicles designed for personal transportation [1]. They include electric scooters, e-bikes, hover boards, and other similar devices that are increasingly popular as a means of short-distance transportation in urban areas. These devices are often powered by rechargeable batteries and can be ridden on sidewalks, bike lanes, and some roads, depending on local regulations [2]. PMDs are used in a variety of real-time scenarios, particularly in urban environments, as they offer an efficient and environmentally friendly alternative to traditional means of transportation. For example, e-bikes and electric scooters are popular for short trips, such as commuting to work, running errands, or traveling short distances within a city. They can help reduce traffic congestion and air pollution, as well as provide a cost-effective and convenient mode of transportation. Additionally, PMDs can be used in large facilities such as airports, theme parks, and universities, where they are often used for short trips between buildings or to cover large distances quickly. They are also increasingly used in logistics and delivery services, where they provide a practical and cost-effective solution for last-mile delivery [3]. PMDs are typically powered by rechargeable batteries that have a limited lifespan. This means that users need to regularly charge their devices to maintain their operability. As PMDs become more popular, the availability of charging infrastructure may become an issue. In many cases, users may not have access to convenient charging stations, which can limit the range and usability of their devices [4][5]. PMDs can be relatively fast-moving and may not always be visible to other road users, which can create safety concerns. In addition, some PMDs may not be designed to handle uneven or challenging terrain, which can increase the risk of accidents. The increasing popularity of PMDs has led to a range of regulatory issues, including questions around where they can be used, who can use them, and how they should be regulated [6]. Overall, addressing these problems is essential to ensure the safe and effective use of PMDs in real-world scenarios.

A charging station for PMDs [7][8] is a specialized facility that allows users to recharge their devices. These charging stations are typically equipped with necessary electrical infrastructure and charging ports that are compatible with a variety of PMDs, such as e-scooters and e-bikes. The charging station may be owned and operated by the manufacturer of the PMD or by a third-party service provider [9]. Charging stations for PMDs play a critical role in enabling the widespread adoption of these devices, as users need to be able to charge their devices conveniently and reliably. They also help to address the issue of limited battery life and range, which can be a significant barrier to the widespread use of PMDs [10][11]. The design of a charging station for PMDs is typically driven by factors such as the power requirements of the devices, the charging time required, and the number of devices that need to be charged simultaneously [12]. Some charging stations may also incorporate additional features, such as Wi-Fi connectivity or the ability to track the location of the devices being charged [13].

One of the significant challenges [14]-[16]in the widespread adoption of PMDs is their charging infrastructure. PMDs such as electric scooters and e-bikes require frequent charging to maintain their battery life and ensure efficient operation. However, the lack of a standardized charging infrastructure and the diversity of battery technologies and charging requirements for different types of PMDs have resulted in a range of challenges. One of the significant challenges is the lack of charging stations in public areas, which leads to range anxiety and limits the usefulness of these devices for daily commuting [17]. Furthermore, the lack of standardization of charging protocols can cause compatibility issues between charging stations and PMDs, making it challenging for users to find charging points and causing unnecessary delays. In addition, many charging stations only support slow charging, which can take several hours to charge the PMD fully, limiting the usability of the devices in areas where the charging infrastructure is not yet fully developed. Another significant problem is the lack of safety and security of charging stations. Unauthorized access to charging stations and the theft of PMDs from charging stations is a significant concern for users[18]. Additionally, poorly designed charging stations can pose safety risks due to improper installation, maintenance, and monitoring. Addressing these problems is essential to the widespread PMDs, and developing efficient, standardized, safe, and accessible charging infrastructure is critical to their success.A smart charging station [19] provides a safe, convenient, and efficient charging solution for PMDs, which can be easily accessible for users. A well-designed charging station can address the shortcomings of existing charging systems for PMDs, such as limited charging voltage range, low charging current ripple, and poor power quality. Smart charging stations can also provide additional features such as real-time monitoring of charging status, remote management, and user authentication [20]. This ensures that the charging process is secure and reliable, and helps to prevent any potential damage to the battery or device. Overall, smart charging stations for PMDs are critical to ensuring the efficient and sustainable operation of these devices. They offer a solution to the problem of insufficient charging infrastructure and help to promote the widespread adoption of PMDs as a clean and efficient mode of transportation.

Our contributions. Our study presents a novel approach towards designing an optimal smart charging station for personal mobility devices, utilizing a multi-level bidirectional DC-DC converter. The main objective of proposed work is to make the charging system more effective and efficient in providing a safe, convenient, and efficient charging solution for PMDs. The key contributions of our proposed work are outlined below.

1. The proposed smart charging station uses a multi-level bidirectional DC-DC converter to interconnect the DC micro-grid with the DC fast charging stations. The converter is designed to address voltage unbalance issues and effectively control the bidirectional power flow. To improve the performance of the converter, a deep multi-graph neural network (DMGNN) is used to optimize the modulation strategy. The DMGNN is capable of learning complex relationships between the input and output variables and providing better accuracy in predicting the optimal modulation strategy. By using DMGNN, the proposed charging system can achieve higher efficiency and lower charging current ripple, which is critical for maintaining the battery life of PMDs.
2. Modified emperor penguin optimization (MEPO) algorithm is used to solve optimization problem of accurately determining the many decision variables during the design of optimal charging stations. It is used to find the optimal values for decision variables such as the number of converter levels, switching frequency, and modulation index. By using the MEPO algorithm, the proposed charging station can achieve higher efficiency and lower cost.
3. Simulations were carried out to test the performance of the proposed charging system under different conditions, such as different charging voltage and current levels, various types of PMDs, and different charging modes. The simulations were performed using software such as MATLAB and Simulink, and the results were analyzed to evaluate the charging efficiency, voltage stability, and ripple current of the charging system.

This paper is structured as follows: Section 2 presents an overview of the related research on charging stations for PMDs using DC-DC converters. In Section 3, we describe the problem methodology and system design of our proposed work. The detailed working process and steps of the proposed system, along with the mathematical models used, are explained in Section 4. Section 5 presents the simulation results and a comparative analysis of our proposed charging system with existing charging systems. Finally, Section 6 concludes the paper.

2. Related works

In this section, we provide a comprehensive understanding of the state-of-the-art research related to charging stations for PMDs. It reviews the recent literature on the topic, including the latest advancements in charging station technology, multi-level converters, and techniques used for designing charging stations.Table 1 presents a summary of the research gaps identified from previous works.

Gabbar et al. [21] proposed to support vehicle electrification, cutting-edge computational intelligence technology employs the Enhanced Artificial Immune System (EAIS).To maintain load balance and avoid grid failure, FFCS is integrated with utility networks, resulting in lower energy costs and increased use of clean energy sources. To improve the FFCS's response, EAIS is used as an advanced optimization technique to fine-tune its dynamic parameters.Lymperopoulos et al. [22] introduced a progressive control component that utilizes the capacity framework of a power transport quick charging framework to offer an extra support (With respect to) the power lattice. The aging, technical viability, and economic viability of storage grid batteries were examined by the authors. Despite the Swiss TSO's regulatory requirements and the fast-charging system's primary purpose of fast-charging buses, the control mechanism demonstrated substantial flexibility in its current configuration. The authors also found that providing AS to the storage network could significantly decrease the energy-related operating costs of the buses. Moreover, the study showed that providing AS did not have a considerable effect on the batteries' aging, indicating that it is a feasible service to integrate without impacting the system's lifetime.

Hou et al. [23], a decentralized charging scheduling system is proposed for standalone charging stations using a formulation of mixed-integer linear programming (MILP). This resolves the issue of consumers' limited charging space and window options. A parallel machine scheduling model is given a continuous solution by mathematical modeling, which incorporates decision variables and constraints. The toll planning problem is solved with an iterative bidding system that is based on game theory and mechanism design. The numerical experiments with an average efficiency of 85% in revealing partial information demonstrate the system's effectiveness in terms of game-theoretic properties like individual rationality and responsiveness to agents.Tao et al. [24] proposed a full-bridge DC/DC converter with a synchronous rectifier and two clamp diodes. On the secondary side of the transformer, terminal diodes were used to reduce switching device losses and suppress voltage fluctuations while also providing switching power to the trailing leg. They dissected the functioning standard and control strategy for the converter and determined the misfortunes of the exchanging gadget. The converter meets the requirements of the integrated charger application by achieving 95 percent efficiency at 20-100% rated load and halving the voltage fluctuations on the secondary side of the transformer.

Li et al. [25] proposed an effective energy move technique between the lattice and an energy stockpiling framework and an enormous accusing station prepared of photovoltaic boards will help EV clients and aggregators. In order to direct PV panels' intermittent system operation, they developed power assignment problems. Based on the aggregator's and EV users' overall satisfaction, an optimized contract capacity algorithm is created for actual operations. Reenactment results show that this calculation gives a few consistently ideal agreement limit sizes contrasted with existing agreement limit power calculations. In Mehrjerdi's study [26], the focus is in Microgrid Long-Term Dynamic Capacity Planning. A microgrid is furnished with different limits like breeze, sun oriented, miniature gas turbine and energy stockpiling framework. As grid vehicles, EVs in a charging station can feed power into the microgrid or alter charging speed and duration, making the station a more adaptable load or generation device. A short-term project is in the process of optimizing the hourly operation of an energy storage system, electric car charging station, and micro turbine. The short-term operation of dispatch resources can effectively contribute to long-term cost reduction planning and reduce planning costs by 28%.

Bayati et al. [27] presented two non-dissipative pulsed current DC-DC and pulsed voltage DC-DC battery charging systems for EV charging stations. To charge and discharge electric vehicles at various voltage levels, the previous design made use of a well-designed control system and a current recirculation unit to generate a negative pulse current. The pulsed voltage method minimizes sudden changes in battery power, making the latter design ideal for high-power applications. The precise design of the control systems in both models ensures that electric vehicles can be charged and discharged effectively.Practical results show that these designs work well and produce less output power ripples and fluctuations than other approaches. Balasundar et al. [28] have proposed Electric vehicle fixed bi-directional charging station with a lithium-ion battery, distribution static compensator, three-phase bi-directional AC-DC converter, and bidirectional chopper. Through bidirectional converters, the system transfers power from the grid to the vehicle and back again. A discrete current and DC voltage control method is used to control a three-phase bidirectional inverter. The bidirectional chopper is controlled by a current control strategy with multiple stages.The framework is assessed utilizing PI and ANFIS regulators in light of DC voltage of appropriation static compensator and lattice current music. The source current THD is reduced and the DC circuit voltage is effectively controlled by the ANFIS controller. EV batteries are shielded from deep discharge and overcharging with a method of multi-stage DC control.

Fescioglu-Unver et al. [29] have developed An EV charging station's resources are controlled by a model called FC-EXP using feedback control. FC-EXP's goal is to maintain the target ratio between the delay times of high and normal priority vehicles while simultaneously providing priority service to high priority vehicles. A charging station sets different dormancy targets in light of its evaluating strategy, and FC-EXP changes asset distribution progressively to meet these objectives. The model is capable of self-monitoring and can be demonstrated to respond to unforeseen events changes in the environment faster than traditional express service models. Numerical analysis indicates that FC-EXP is effective in achieving its goals both in real-time and in steady-state conditions.Leal et al. [30] have introduced a DC-DC converter with a step-down bidirectional interleaved design that can be used in electric vehicle charging stations and supports both grid-to-vehicle (G2V) and vehicle-to-grid (V2G) technologies.The EV battery's current ripple, which can either consume or generate power for the microgrid, is reduced using a coupling technique. Using the small signal technique, EV battery charging and discharging are controlled by PI controllers. The experimental outcomes affirm that the equipment arrangement used to test the control design and inverter activity is protected, practical and dependable. This arrangement permitted high current testing without compromising the high current burdens of a genuine EV battery.

Table 1 Summary of Research Gaps

Ref.	Methodology	Techniques used	Findings	Research gaps
[21]	Flywheel fast charging system (FFCS)	Enhanced artificial immune system (EAIS)	Torque, angular speed and energy storage	The DC-DC converter aspect is not the main focus.
[22]	Fast-charging stations for electrical buses	ABB and TOSA	State of battery health	The source current THD level does not meet the necessary standards.
[23]	E-vehicle charging station scheduling	Mixed-integer linear program (MILP)	Efficiency, information revelation	This may result in power quality issues or instability.
[24]	Onboard charging for E-vehicle	Phase-shifted full-bridge DC/DC converter	Transformer ratio, switching frequency	Charging rates may vary due to fluctuations in battery temperature.
[25]	Storage system for E-vehicle charging	Time-of-use adjustment method	Contract capacity, charging cost	The devices are cumbersome to carry due to their size and weight.
[26]	Dynamic and multi-stage capacity expansion	Deep learning with optimization algorithm	Planning cost, Expansion cost	They are not well-suited for use in PMDs.
[27]	DC–DC stage of E-vehicle charging stations	Two battery charging systems	AC-side terminal current	There is no emphasis on minimizing prediction errors.
[28]	Enhanced bidirectional E-vehicle charging station	Multi-step current control strategy	THD, source and load currents	There is a significant amount of switching loss and noise interference.
[29]	Resource management model for charging station	Feedback controlled express station(FC-EXP)	Relative delay	Soft switching cannot be achieved under light loads.
[30]	Converter for gridtovehicleand vehicleto grid	Cascaded interleaved DC–DC converter	Flexibility, converter behavior	The use of pulse voltage can cause pulse current in the battery impedance.

3. Problem methodology and System design

3.1 Research Gaps

A multi-level charging topology is needed for E-Mobility charging stations due to the increasing demand for fast and convenient charging of electric vehicles (EVs). With the growing popularity of EVs, it is becoming increasingly important to have charging infrastructure that can meet the changing requirements of a large number of EVs. Multi-level charging topology allows multiple EVs to be charged simultaneously at different power levels, which can reduce the charging time and improve the utilization of charging stations. It also provides flexibility in charging options for different types of EVs, as some may require faster charging than others. Additionally, multi-level charging topology can help manage the power demand and reduce the load on the power grid by dynamically adjusting the charging rates based on the availability of grid power. Overall, multi-level charging topology is essential for meeting the changing needs of a growing fleet of EVs and supporting the transition to a sustainable transportation system. Lim et al. [31] introduced a multi-level charging topology the minimal expense utilization of an air conditioner/DC converter in large scale manufacturing empowers the power unit to meet the different charging needs of e-portability gadgets. In contrast to conventional charging systems, this one produces less charging current ripple and reduces the sensitivity of input current to THD in relation to output power and voltage. The staggered charging framework's switching method ensures low power loss, reduced switching device voltage stress, and low EMI noise generation. The effectiveness of the charging system was confirmed through simulations using PSIM and experimental testing of a 1200-W charging system.

There are several problems that occur in EV smart charging stations, including: PMDs smart charging stations can experience overloading, particularly during peak hours, which can lead to slow charging, reduced efficiency, and potential damage to the station [21]. If the charging station is not designed efficiently, it can result in power losses [22][23], which can increase the overall charging time and reduce the station's reliability. Not all electric vehicles have the same charging requirements, which can make it difficult for charging stations [22][25] to be universally compatible with all EV models [24]. This can cause inconvenience for EV owners and reduce the utilization rate of charging stations. Long charging times can be a major issue, particularly for drivers who are in a hurry. This can lead to frustration, reduced station utilization, and a negative impact on the overall EV charging experience [26][29]. The cost of installing and maintaining EV smart charging stations can be high, which can deter organizations and individuals from investing in them [23][26]. However, it also notes that the charging systems for PMDs are insufficient compared to those available for EVs. This implies that there is a need for the development of charging infrastructure that is specifically designed to cater to the charging requirements of PMDs, which is currently lacking [28]. The use of a Multi-Level DC/DC Converter in EV smart charging stations can address some of these problems by increasing charging efficiency, reducing charging time, and providing compatibility with different EV models [30]. However, the multi-level converters face some problems related to complex control, and high number of components. Based on the identified research gaps in the area of smart charging stations for personal mobility devices, the following research objectives can be proposed:

1. To design and develop a smart charging system that can accommodate different types of PMDs.
2. Streamline the charging system to decrease the charging time and increment the effectiveness of the charging framework.
3. To design an efficient multi-level converter to regulate the DC voltage and current to ensure safe and efficient charging of the EV battery.
4. To ensure the safety of the charging system by implementing appropriate measures to prevent overcharging and overheating.
5. To reduce the reliance on fossil fuels and minimize the negative impact on the environment by incorporating renewable energy sources into the charging system.
6. To develop a communication network between the charging station and PMDs to enable real-time monitoring and control of the charging process.
7. To validate the smart charging system's effectiveness in meeting PMDs' needs by evaluating its performance through simulations and experiments.

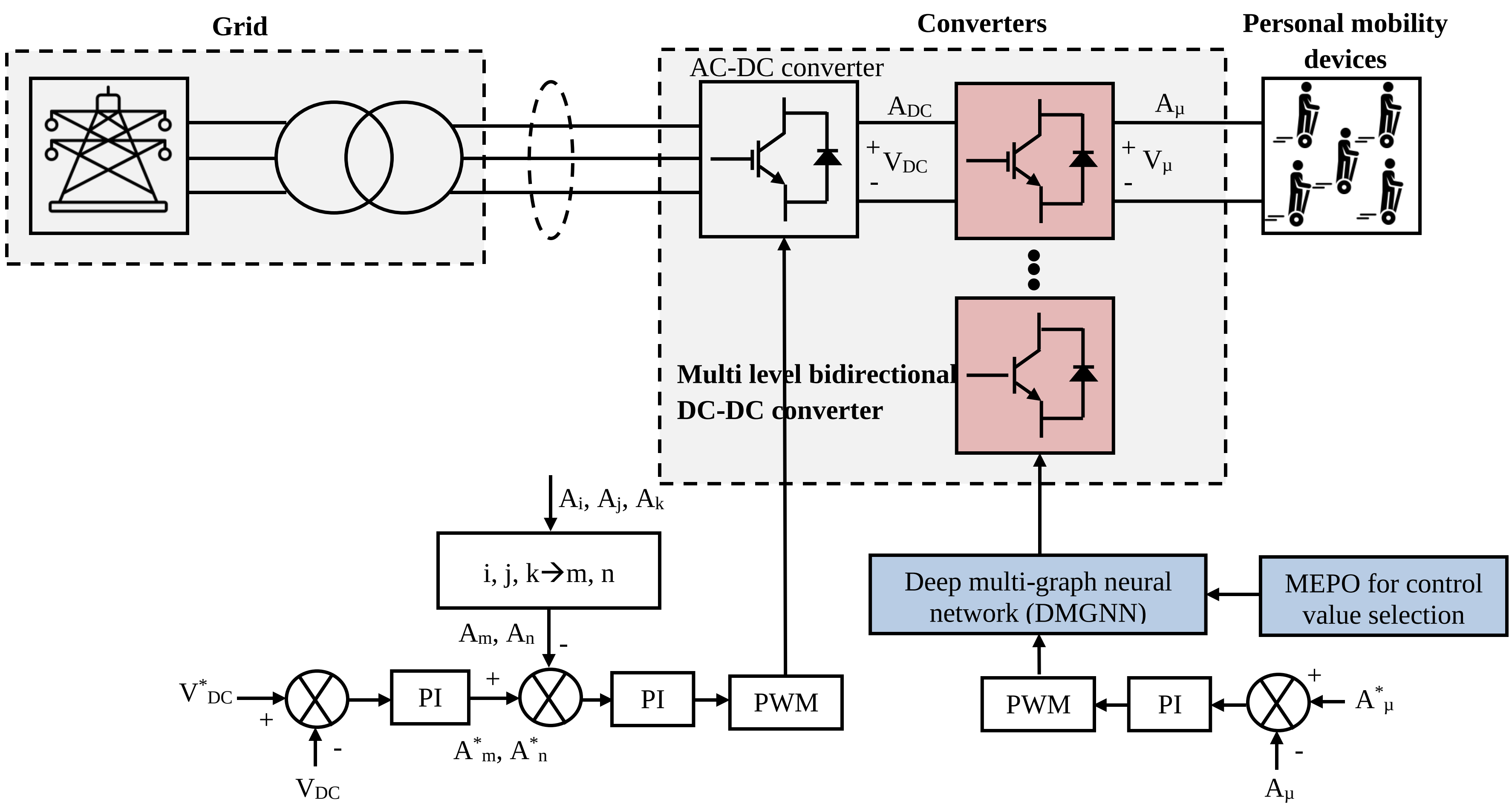

Fig. 1 Overall system design of our proposed work

3.2 System design of proposed work

The DC supply voltage for charging small electric vehicles like electric scooters must be less than 60 V, according to Korea's technical regulations for products and components in the electrical and telecommunications industries. A smart charging system was proposed to meet the requirement for charging systems that can generate voltage greater than 60 V to charge E mobility equipment of varying voltages.As depicted in Fig. 1, the framework uses staggered bidirectional DC converters associated in series, where the result voltage Vμ of every converter covers.A voltage that can drive a general gate amplifier is used for each level of the converter's input voltage, Ai, Aj, and Ak. The system configuration uses a field-effect transistor (FET) switch to make use of the gate amplifier voltage as the power supply voltage, connect An to the negative terminal of the input power supply Am. The proposed staggered converter's result voltage can be constrained by the state and obligation proportion of the switch arranged in the framework. In the proposed smart charging station for PMDs, a DMGNN is used to enable the multi-level bidirectional DC-DC converter to interconnect the DC micro-grid with the DC fast charging stations. DMGNN helps to address voltage unbalance issues and effectively control the bidirectional power flow. The DMGNN is used to predict the voltage of each level of the staggered converter and balance the voltage among them, thereby improving the converter's performance. Additionally, the DMGNN is used to determine the optimal duty ratios of the switches in the converter, which helps to achieve higher efficiency and a wider charging voltage range in the low output voltage region. Overall, the use of DMGNN in the proposed charging system helps to achieve higher efficiency, lower charging current ripple, and a wider charging voltage range. The modified emperor penguin optimization (MEPO) algorithm is used in this case to solve the optimization problem of accurately determining the many decision variables during the design of optimal charging stations. MEPO algorithm is particularly suitable for this case because of its ability to optimize a large number of variables simultaneously while ensuring the optimal solution is found within a reasonable time. Moreover, it has been shown to be effective in solving complex engineering problems with multiple constraints and objectives. By using MEPO, the proposed charging system can be optimized to ensure It achieves high efficiency while maintaining a low charging current ripple and meeting the voltage requirements of a variety of E-mobility devices.

4. Proposed Methodology

In this section, we will introduce the proposed methodology for our smart charging system. Firstly, we will explain the structure of the multi-level bidirectional DC-DC converter and its activities. We will then discuss the control system utilizing the DMGNN technique. Finally, we will explain the working process of the MEPO algorithm, which is an essential component of our proposed methodology.

4.1 Multi-level bidirectional DC-DC converter

The proposed smart charging system for PMDs makes use of a multi-level bidirectional DC-DC converter that consists of independent converters connected in series. The result voltage of every converter is covered to accomplish the required charging voltage. A voltage that can drive a general gate amplifier is used for each level of the converter's input voltage. The system configuration uses a field-effect transistor (FET) switch in the negative terminal of the input power supply to use the gate amplifier voltage as the power supply voltage. Figure depicts the structure of a bidirectional DC-DC converter with multiple levels. 2. B1, B2, B3, and B4 are the primary switches on the weight side, which empower the buck-support activity through various information force of each level in the staggered converter addressed by VjMLDC, and the amount of the voltage as per the exchanging condition of the staggered converter addressed by VMLDC. The energy that can be transferred from the source to the storage system determines when the switches turn ON and OFF, as well as the effort required to implement a unidirectional current flow between the connected switching devices. A buck-boost converter is connected in series by the multi-level bidirectional converter [31]. Consequently, the buck converter's characteristics were first investigated. A regular buck converter's voltage, recurrence, and obligation proportion decide the inductor current wave. The inductor current ripple (Mr) is determined by the voltage ripple of the output voltage and the current ripple of the inductor (L). Assuming the ongoing AL, the current ripple caused by the inductor, is what is meant to be coursing through it. γ_{AL} is expressed as follows.

$$\gamma_{AL} = \frac{Mr}{L} V_j C \left(1 - C\right) \tag{1}$$

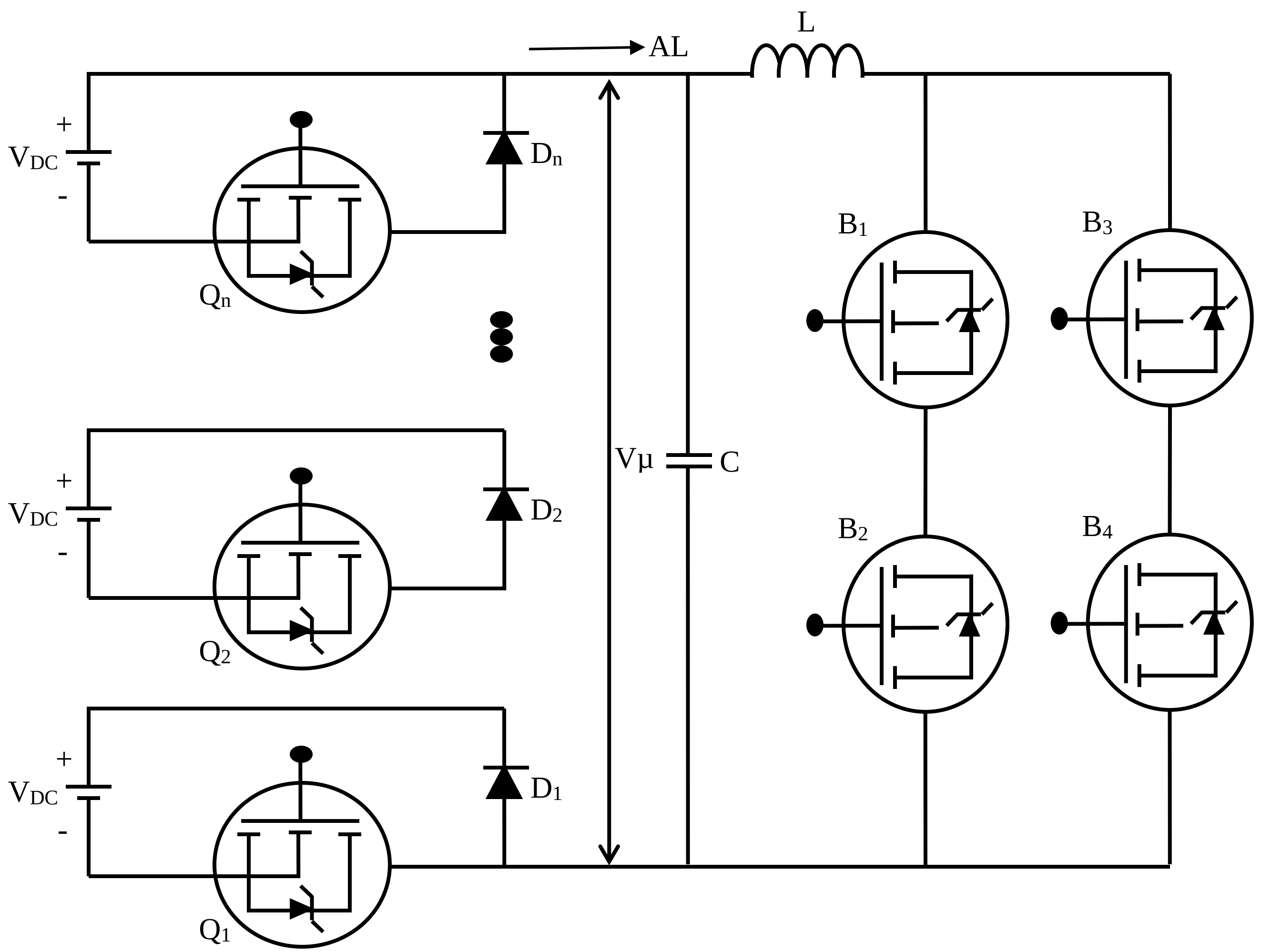

Fig. 2 Structure of multi-level bidirectional DC-DC converter

Similarly, the output voltage $V_{out}$is connected with the information voltage Vin and the obligation factor d. The voltage wave of the result voltage is relative to the result current and equivalent to the series opposition of the inductor. The ripple is smoothed out by a capacitor on the output side, whose value is determined by the allowable ripple and load current. It is essential to comprehend these characteristics conduct of the buck-help converter and planning the staggered bidirectional converter.

$$\gamma_{A_{Vout}} = \frac{V_j C (1 - C) M_r^2}{8LC} \tag{2}$$

The proposed multi-level converter's current and voltage the converter's duty ratio and number of levels in comparison to a standard determine ripple buck-boost converter. When the number of levels in the proposed converter equals the maximum ripple value in a conventional buck-boost converter, this is the maximum ripple condition. During the charging mode, the proposed converter acts as a reducing converter, transferring energy via a DC voltage transfer function from the DC bus to the storage units. The multi-level converter's input voltage, which is made up of N numbers, is called VjMLDC. It is determined how many levels, or NMLDC, are necessary to generate the output voltage, Vout, VjMLDC, derived from the input voltage. The number of converters that use pulse width modulation (PWM) between 0 and duty 1 is referred to as NMLDC. If the converter's switching state is duty, the number of converters performing PWM is not counted. The duty ratios of the output voltages, Vout and CMLDC, can be expressed using this definition.

$$V_{out} = V_{jMLDC} \left(N_{MLBD} + (C_{MLBD} - 1) N_{MLBD} \right) \tag{3}$$

$$C_{MLBD} = V_{out} - \left(\frac{V_{jMLBD} * (N_{MLBD} - 1)}{V_{jMLBD} * N_{MLBD}} \right) \tag{4}$$

The current ripple generated by each level in the multi-level converter can be canceled out by using the overlapping effect of the output voltages from each level. When the output voltage of one level decreases, the output voltage of the adjacent level increases, and the two voltages overlap each other, resulting in the cancellation of the current ripple. This overlapping effect γ_{AL}

is achieved by controlling the duty ratio of each switch in the converter, which adjusts the output voltage of each level.

$$Cancel\gamma_{AL} = \frac{N_{MLBD}\left(C_{MLBD} - \frac{N_{MLBD} * C_{MLBD}}{N_{MLBD}}\right)\left(\frac{\left(N_{MLBD} * C_{MLBD}\right)+1}{N_{MLBD}} - C_{MLBD}\right)}{C_{MLBD}\left(1 - C_{MLBD}\right)} \tag{5}$$

By adjusting the duty ratio, the overlapping effect can be maximized, and the current ripple can be minimized. This results in a smoother output voltage and a more efficient charging process for E-mobility devices.

4.2 Bidirectional power flow controller using DMGNN

The deep multi-graph neural network (DMGNN) is used to control the bidirectional power flow in the proposed multi-level bidirectional DC-DC converter. DMGNN technique is used to design a control system that can effectively address voltage unbalance issues and keep the charging current ripple at a low level. It allows for the optimal operation of the converter, taking into account various parameters such as the input and output voltages, the switching states of the converters, and the duty ratios of the output voltages. DMGNN is trained on a large dataset of simulation results, allowing it to accurately predict the optimal control parameters for a given set of inputs. This approach results in a highly efficient and effective control system for the proposed charging station, capable of charging a range of E-mobility devices while maintaining a low current ripple. DMGNN is a type of neural network architecture used for tasks that involve structured data with multiple graphs. DMGNNs can be thought of as an extension of graph neural networks (GNNs) that can handle multiple graphs, where each graph represents a different aspect or relationship in the data. DMGNNs use multiple graph convolutional layers to extract features from each graph independently, and then combine them to make a final prediction. Each graph convolutional layer operates on a single graph, using the graph's adjacency matrix to compute node representations. By stacking multiple such layers and aggregating the node features across graphs, DMGNNs can learn complex relationships between different aspects of the data. Specifically, the DMGNN is used as a controller to regulate the output voltage and current of the converter in both the buck and boost modes. The DMGNN takes the input signals of the converter, such as the output voltage, current, and reference voltage, as well as the switching states of the converter as its inputs. It then processes these inputs using multiple layers of graph neural networks, which allows it to learn the nonlinear relationships between the inputs and outputs of the converter. DMGNN is trained using a dataset that consists of input-output pairs generated by simulating the behavior of the converter under various operating conditions. During training, the DMGNN adjusts its parameters to minimize the difference between its predicted outputs and the actual outputs of the converter. Once the DMGNN is trained, it can be used to control the converter in real-time by predicting the optimal switching states based on the current operating conditions. This allows for precise and efficient control of the converter, even under varying load and input conditions. DMGNN typically consists of multiple layers, each of which performs a specific type of computation. The exact number and types of layers used can vary depending on the specific application and requirements. However, in general, a DMGNN consists of three main types of layers: graph convolutional layers, pooling layers, and fully connected layers.

- Graph convolutional layers are used to perform convolutional operations on the input graph. They take the node features and the graph structure as inputs and produce a set of node features as output.
- Pooling layers are used to aggregate the node features over different regions of the input graph. They take the node features and the graph structure as inputs and produce a set of aggregated node features as output.
- Fully connected layers are used to perform linear transformations on the aggregated node features. They take the aggregated node features as inputs and produce a set of output features that can be used for classification or regression.

The mathematical model of DMGNN is start with the dimension of the data features, which can be optimizes as follows.

$$Dim(A_{lstm\_out}) = Int\left(\frac{Dim(A_{input})}{2}\right) \tag{6}$$

where A_{lstm_out} and A_{input} are the input and output of the DMGNN which includes the number of hidden layers, data flow and settings. To defines the MinMaxScaler normalization by using following pre-processing.

$$a_I = \frac{a_I - a_{Min}}{a_{Max} - a_{Min}} \tag{7}$$

where a_{Max} and a_{Min} are the maximum and minimum values of the dataset input vector. Then, we utilize the GNN with double XG boosting for hidden layer design and optimization of it. First, we formulate the mathematical theory behind it and assume an input $W \times G$, given features, $\mathrm{l} \in \mathrm{R}^{\mathrm{w} \times \mathrm{g}}$, represented as follows:

$$l = \{b(P,Q) \,|\, 1 \le P \le W, 1 \le Q \le g\} \tag{8}$$

where $b(P,Q)$ is the intensity of the input P,Q and, given the $w_K \times g_K$ filters, K is a convolution that uses the input, l, and the filter K to produce a feature map B. On the K input, a filter with a padding value of L phase T_K and zero sweeps.

$$(l \otimes K)_{P,Q} = \sum_{u=-w_K}^{w_K} \sum_{v=-g_K}^{g_K} K_{U,V} \, i_{P+u,i+v} \tag{9}$$

The input applies a convolution operation and an additional offset to the feature map at each convolutional layer indexed by L, which is indexed by the jth feature $F \in \{1,...,F(l)\}$.map output $a_J^{(l)}$ of the jth layer. From the result of the $a_J^{(l)}$ past layer

$$a_J^{(l)} = \phi\left(X_J^{(l)} + \sum_{I=1}^{F^{(l-1)}} k_{J,i}^{(l)} * b_J^{(l-1)} \right) \tag{10}$$

$$a_J^{(l)} = \phi\left(X_J^{(l)} + \sum_{I=1}^{F^{(l-1)}} k_{J,i}^{(l)} * b_J^{(l-1)} \right) \tag{11}$$

where F is the magnitude filter, the shift matrix, and the activation function $X_j^i$for the rectified kj,ilinear unit $2W_k+1\times 2g_k+1$ of ReLU. Thus the result components of layer l for the element map at position.

$$(a_j^{(l)})_{P,Q} = \phi\left(\left(X_J^{(l)}\right)_{P,Q} + \sum_{J=1}^{F^{(l-1)}} \left(k_{J,i}^{(l)} \otimes b_J^{(l-1)}\right)_{P,Q} \right) \tag{12}$$

$$= \phi\left(\left(X_J^{(l)}\right)_{P,Q} + \sum_{I=1}^{F^{(l-1)}} \sum_{u=-w_K^{(l)}}^{F^{(l-1)}} \sum_{i=1}^{F^{(l-1)}} \left(k_{J,I}^{(l)}\right)_{P,Q} \left(b_J^{(l-1)}\right)_{P+u,Q+v} \right) \tag{13}$$

The output of the layer is further modified by a concatenation layer: It prevents the output from being overfitted and reduces sampling. For instance, a pooling process with steps and a pooling window is used to process an output from the previous layer that has an activation function f, which is a pooling function.

$$N(a_j^{(l)})_{P,Q} = \max\left(a_J^{(l)}\right)_{P,Q} \tag{14}$$

The following is how the maximum pooling window is affected by the optimal function:

$$DN(a_j^{(l)})_{P,Q} = \left((w - w_K)/T_q + 1\right) \times \left((G - g_K)/T_q + 1\right) \tag{15}$$

The final layer of the DMGNN architecture is the fully pooled layer, whose input is the column vector because the output of the pooling layer before it is extended. Algorithm 1 describes the working steps involved in the process of bidirectional power flow controller using DMGNN.

Algorithm 1 Bidirectional power flow controller using DMGNN

Input	: A_μ, A^*_μ, PWM signal and termination condition
Output	: Power flow controller
1	Initialize MainNet with random values
2	Define the features data dimension $Dim(A_{lstm\_out}) = Int\left(\frac{Dim(A_{input})}{2}\right)$
3	Compute MinMax scalar normalization
4	While j=0 Do
5	For $s=1$, S do

6 Define input range for input layer $l \in R^{w \times g}$ $l = \{b(P,Q) \mid 1 \le P \le W, 1 \le Q \le g\}$

7 Compute output of the previous layer $a_J^{(l)} = \phi\left(X_J^{(l)} + \sum_{I=1}^{F^{(l-1)}} k_{J,i}^{(l)} * b_J^{(l-1)} \right)$

8 Compute max-pooling window of dimension
$DN(a_j^{(l)})_{P,Q} = \left((w - w_K)/T_q + 1\right) \times \left((G - g_K)/T_q + 1\right)$

9 End if

10 Update the final values

11 End

4.3 Compute decision variables using MEPO algorithm

The modified emperor penguin optimization (MEPO) algorithm is a metaheuristic optimization algorithm that is used in this work to advance the control boundaries of the staggered bidirectional DC converter. The fundamental job of the MEPO calculation is to find the ideal qualities for the control boundaries that can limit the mistake between the real result voltage and the ideal result voltage of the converter. MEPO has inspired by the behavior of emperor penguins in Antarctica, where they use different strategies to communicate and navigate in a harsh environment. The algorithm works by simulating the movements and interactions of penguins in the search for food and mates. MEPO algorithm is known for its ability to find the global optimal solution with high degree of accuracy, even in complex and high-dimensional optimization problems.

In this work, MEPO is used to optimize the duty ratios and switching frequency of the multi-level bidirectional DC-DC converter. MEPO algorithm consists of several steps. First, an initial population of potential solutions is generated randomly. Each solution is represented as a set of parameters for the DMGNN control system. These parameters include weights, biases, and connection strengths of the neural network. Next, the fitness of each solution is evaluated based on its ability to control the multi-level bidirectional DC-DC converter. It is done by simulating the behavior of the converter using the current set of parameters and measuring the performance of the control system in terms of several performance metrics.After the fitness evaluation, a selection process is performed to choose the best-performing solutions. The selected solutions are then used to generate new candidate solutions through hybrid and transformation tasks. Mutation, on the other hand, is the process of combining two solutions to create a new one.

randomly changing the parameters of a solution. The new candidate solutions are evaluated for their fitness, and the process is repeated for a certain number of generations or until a satisfactory solution is found. The algorithm also includes several parameters that control the selection pressure, mutation rate, and crossover rate. MEPO algorithm has been shown to be effective in optimizing the parameters of the DMGNN control system for the multi-level bidirectional DC-DC converter. It allows for efficient training of the control system, and the resulting solutions are often superior to those obtained through other optimization methods.Assume that the wind gradient and velocity is compute as follows.

$$\rho = \perp \alpha \tag{12}$$

$$R = \alpha + o\eta \tag{13}$$

where α is random vector and η is an imaginary constant. The penguin's position will change randomly based on the penguin's best position. A penguin in the middle of an L-shaped polygon fits your best. To survive the winter, penguins conserve heat in groups. If polygon radius (R) is greater than 1, temperature (t) is assumed to be set to 0. Otherwise, temperature (t) is set to 1. The difference between the pool temperature and the temperature outside the pool boundary (T) is calculated as follows.

$$E = \left(e - \frac{Max_{iteration}}{z - Max_{iteration}} \right) \tag{14}$$

$$t = \begin{cases} 0, P \geq 1 \\ 1, P \leq 1 \end{cases} \tag{15}$$

Where x is the current frequency and t is the temperature profile. The key to finding other emperor penguins is the best emperor penguin. All other Imperial Penguin' positions will be changed correspondingly.

$$\vec{S} = Dfw\left(F\left(\vec{U}\right)\vec{X}(w) - C\,\overrightarrow{Dfr}(w)\right) \tag{16}$$

where Y and Z are used to avoid collisions between emperor penguins. Dis represents the distance between the emperor penguin and the top emperor penguin. The current iteration is Rs.

Q represents the top penguin-→Qep represents the position of the sovereign penguin. The social power emperor penguins use to find the best solution is called b ().

$$\vec{U} = \left(M \times \left(E + X_{grid}\left(Accuracy\right)\right) \times Rand(\ )\right) - E \tag{17}$$

$$X_{grid}\left(Accuracy\right) = Dfw\left(\vec{X} - \overrightarrow{Xwr}\right) \tag{18}$$

$$\vec{C} = Rand(\ ) \tag{19}$$

A motion parameter N with a value of 2 is used to isolate penguins. The precision of the polygon grid is expressed as qgrid and the random function rand () takes values between [0, 1].

$$\overline{Y\left(\vec{U}\right)} = \sqrt{\left(h\,q^{-w}y - q^{-w}\right)^2} \tag{20}$$

Here e is expression characteristic and g and l are control limits and their values are in the range [2, 3] and [1.5, 2] respectively. Emperor penguin mod is updated based on the best emperor penguin engine.

$$\overrightarrow{Xfr}\left(W+1\right) = \vec{X}\left(W\right) - \vec{U}.\vec{S} \tag{21}$$

whereQep(s + 1) is optimal solution while repeating this the penguin changes position. The optimal penguin position is recalculated during the movement of the penguin pack. The working process of decision variables computation using MEPO is describes in Algorithm 2.

Algorithm 2 Decision variables computation using MEPO

Input	: duty ratios, switching frequency and maximum iteration
Output	: decision variables
1	Initializes the total population
2	Define wind gradient and velocity using $\rho = \perp \alpha$ and $R = \alpha + o\eta$
3	For P>1
4	Compute optimal pool boundary using $E = \left(e - \frac{Max_{iteration}}{z - Max_{iteration}}\right)$

Compute initial fitness function using $\vec{S} = Dfw\left(F\left(\vec{U}\right)\vec{X}(w) - C\,\overrightarrow{Dfr}(w)\right)$

Define Upper and lower limits

Otherwise update the best solution as last iteration solution

Perform rule updating process to compute precision

Update the best solution using $\overrightarrow{Y(U)} = \sqrt{\left(h\,q^{-w}y - q^{-w}\right)^2}$

Define moving point of emperor penguin using $\overrightarrow{Xfr}(W+1) = \vec{X}(W) - \vec{U}.\vec{S}$

Final fitness = moving point of emperor penguin

End for

End

5. Results and Discussion

In this section, we present the results of simulations and provide a comparative analysis between their proposed bidirectional DC-DC converter with multiple levels and the existing converters for charging systems. MATLAB Simulink was used for the simulations, and various scenarios were tested to evaluate the converters' performance. The voltage, right off the bat, was expanded straightly to determine the inductor current wave and the resulting voltage from 0 V to 70 V. swell in every voltage locale. To ensure a fair comparison of the inductor's current, the inductance value was set to the lowest value necessary for continuous flow.The proposed was contrasted with the multi-level converter and conventional buck converter multi-level bidirectional DC-DC converter [31]. Table 2 gives details to the reproduction circuit used to test the proposed staggered bidirectional DC-DC converter. The converter input voltage is set to 12 V, while the output inductor has an inductance value of 200 μH. The output capacitor has a capacitance value of 10 μH, and the output load resistance is set to 600Ω. The switching frequency used in the simulation is 20 kHz. These parameters were selected based on the requirements of the proposed charging system and the capabilities of the simulation software. The values are important to ensure that the simulation accurately reflects the performance of the converter in the proposed charging system. By using these parameters, the simulation can be used to evaluate the efficiency and effectiveness of the proposed converter in meeting the charging voltage requirements of personal mobility devices while keeping the charging current ripple at a low level.

Table 2 Specifications of proposed simulation circuit

Parameter	Value
Converter input voltage	12 V
Output inductor inductance	200 µH
Output capacitor capacitance	10 µH
Output load resistance	600Ω
Switching frequency	20 kHz

Fig. 3 shows the recreation circuit plan of the proposed staggered bidirectional DC converter. The circuit is made up of three H-bridges that are connected in series. Each H-bridge has two diodes (D1 and D2) and four switches (S1, S2, S3, and S4). A controller's pulse width modulation (PWM) signal is what drives the switches. The DC source is connected to the middle H-bridge, while the left and right H-bridges are connected to the load and the battery, respectively. The proposed converter also includes an LC filter, which consists of an inductor and a capacitor, to reduce the output voltage ripple. The simulation circuit is designed using MATLAB Simulink and SimPowerSystems. Fig. 4 shows the PWM level shift control using DMGNN. The DMGNN controller is used to adjust the duty cycle of the switches to regulate the output voltage and current. It includes several layers of neural networks that can learn the complex relationships between the input voltage and current and the output voltage and current. DMGNN controller is trained using simulation data to achieve optimal control of the bidirectional power flow in the charging system. The output of the DMGNN is the duty cycle of the switches, which is fed to the gate driver circuit. The gate driver circuit generates the appropriate signals to control the switches. By changing the obligation pattern of the switches, the PMD have some control over the result voltage and current to give the right charging voltage and current. Figure 5 shows the exhibition aftereffects of the proposed staggered bidirectional DC converter. Figures (a) and (b) address the arm voltages, where (b) is an extended perspective on (a) to show the voltage waveforms plainly. Similarly, subfigures (c) and (d) depict the pole voltage, with (d) being an enlarged view of (c). The x-axis in each subfigure represents the simulation time, while the y-axis represents the voltage amplitude in volts. These plots were obtained through simulation using the proposed simulation circuit and MATLAB Simulink.

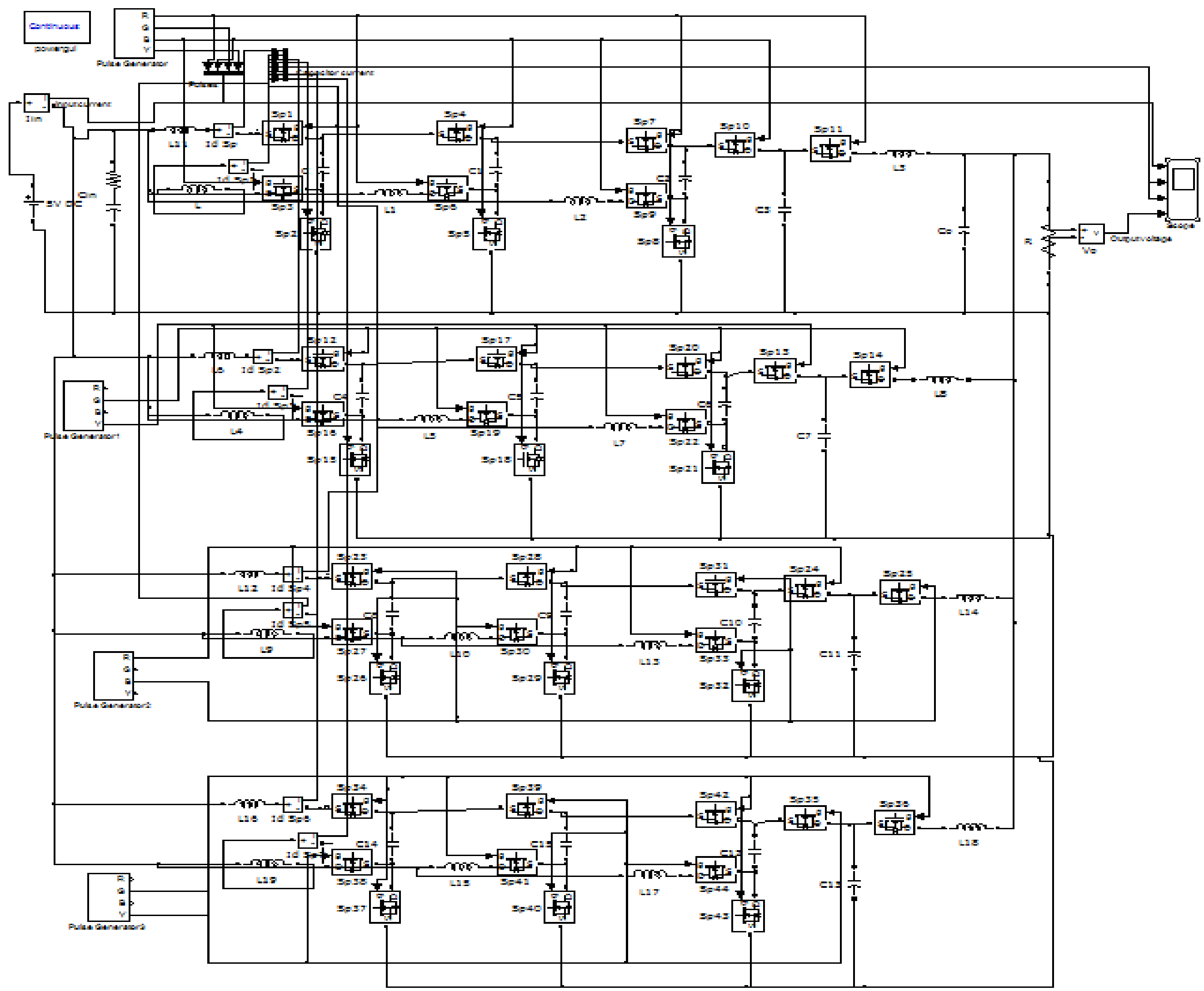

Fig. 3 Simulation circuit design of proposed multi-level bidirectional DC-DC converter

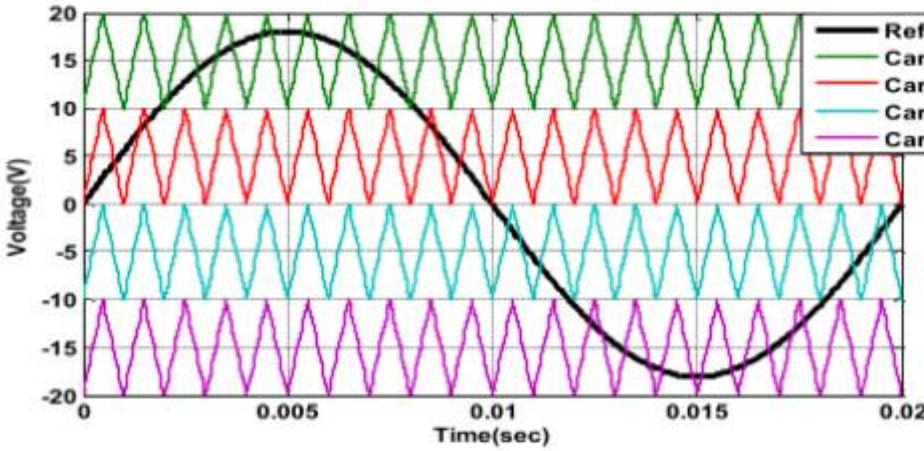

Fig. 4 PWM level shift control using DMGNN

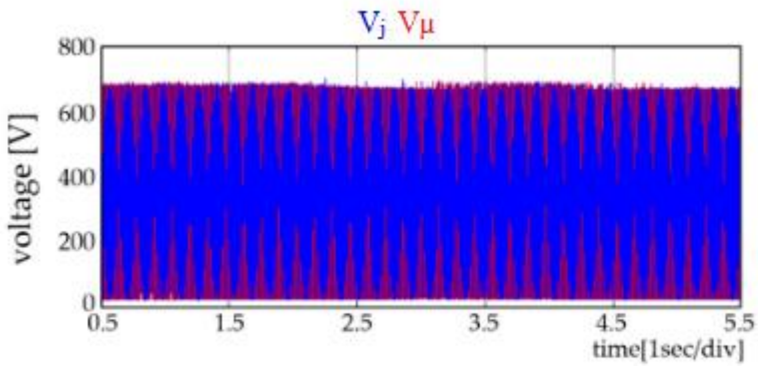

(a)

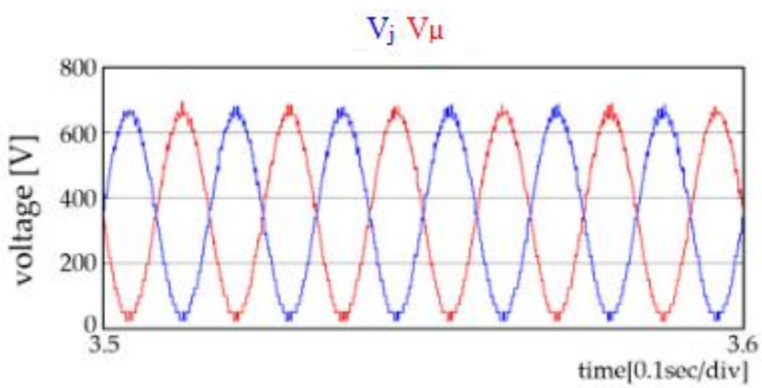

(b)

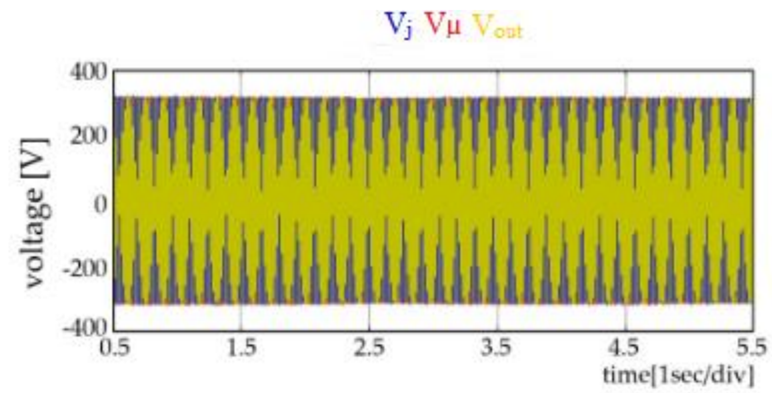

(c)

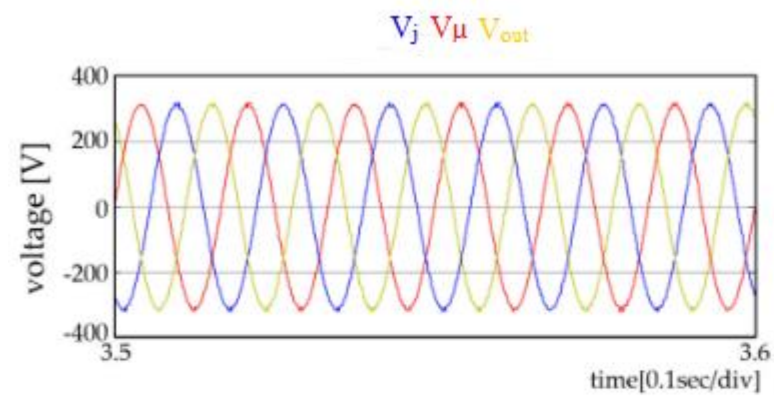

(d)

Fig. 5 Characteristic results of proposed multi-level bidirectional DC-DC converter with (a) arm voltage (b) enlarged arm voltage (c) pole voltage (d) enlarged pole voltage

5.1 Comparative analysis with respect to current ripple

Table 3 presents a comparative analysis of the current ripple (γAL) in Amperes (A) for the proposed multi-level bidirectional DC-DC converter (MLDC) and an existing converter design (MLd) at varying input voltages and number of converters (N_{MLDC}). The results indicate that with an increase in the number of converters, the current ripple decreases for both MLDC and MLd designs. However, the proposed MLDC design consistently outperforms the existing MLd design, with a lower current ripple at all tested input voltages and numbers of converters. For instance, at an input voltage of 10V, when N_{MLDC} is equal to 1, the current ripple for the proposed MLDC is 5.551A, which is approximately 4.3% lower than the existing MLd design. As the number of converters increases, the percentage decrease in the current ripple for the proposed MLDC compared to the existing MLd design becomes more significant. At N_{MLDC}=10, the current ripple for the proposed MLDC is 0.277A, which is approximately 45.9% lower than the current ripple of 0.512A for the existing MLd design.The reduction in current ripple is significant and ranges from 4.3% to 45.9% lower compared to the existing design. For instance, at an input voltage of 20V and with one converter performing PWM (N_{MLDC}=1), the current ripple for the proposed converter is 6.119 A, which is 3.8% lower than that of the MLd (6.354 A). Furthermore, as the number of converters performing PWM increases, the current ripple decreases for both converters. However, the proposed converter consistently exhibits lower current ripple values than the MLd. For example, at an input voltage of 20 V and with ten converters performing PWM (N_{MLDC}=10), the current ripple for the proposed converter is 0.845 A, which is 21.7% lower than that of the MLd (1.080 A). For V_{IN}=30V, the proposed converter design (MLDC) once again shows a lower current ripple than the existing design (MLd) at all levels of N_{MLDC}. The highest difference in current ripple is observed at NMLDC=1, where the proposed converter design shows a 3.6% decrease in current ripple compared to the existing design. As N_{MLDC} increases, the difference in current ripple between the two designs decreases, with the proposed design showing a 50.8% decrease in current ripple at N_{MLDC}=10.

The current ripple of the proposed MLDC is lower than that of the existing MLd design for all values of N_{MLDC}, ranging from 1 to 10. For N_{MLDC}=1, the current ripple of the proposed MLDC is 3.39% lower than that of the existing MLd design. For N_{MLDC}=2, the current ripple of the proposed MLDC is 6.02% lower than that of the existing MLd design. As the number of converters increases, the percentage decrease in the current ripple of the proposed MLDC compared to the existing MLd design also increases. For NMLDC=10, the current ripple of the proposed MLDC is 10.62% lower than that of the existing MLd design. For input voltage of 50V, comparing the results for N_{MLDC}=1, the current ripple for MLDC converter is 7.823 A, which is 1.43% less than the MLd converter's value of 8.058 A. For N_{MLDC}=5, the current ripple for MLDC converter is 2.947 A, which is 7.43% less than the MLd converter's value of 3.182 A. Similarly, for N_{MLDC}=10, the current ripple for MLDC converter is 2.549 A, which is 8.31% less than the MLd converter's value of 2.784 A.

Table 3 Current ripple (γ_{AL}) (A) comparative analysis of proposed and existing converters design with varying input voltage and number of converters (N_{MLDC})

Number of converters (N_{MLDC})	**Input voltage (V_{IN})**									
	10		**20**		**30**		**40**		**50**	
	MLd [31]	**MLDC**	**MLd [31]**	**MLDC**	**MLd [31]**	**MLDC**	**MLd [31]**	**MLDC**	**MLd [31]**	**MLDC**
1	5.786	5.551	6.354	6.119	6.922	6.687	7.490	7.255	8.058	7.823
2	2.148	1.913	2.716	2.481	3.284	3.049	3.852	3.617	4.420	4.185
3	1.448	1.213	2.016	1.781	2.584	2.349	3.152	2.917	3.720	3.485
4	1.030	0.795	1.598	1.363	2.166	1.931	2.734	2.499	3.302	3.067
5	0.910	0.675	1.478	1.243	2.046	1.811	2.614	2.379	3.182	2.947
6	0.792	0.557	1.360	1.125	1.928	1.693	2.496	2.261	3.064	2.829
7	0.652	0.417	1.220	0.985	1.788	1.553	2.356	2.121	2.924	2.689
8	0.623	0.388	1.191	0.956	1.759	1.524	2.327	2.092	2.895	2.660
9	0.598	0.363	1.166	0.931	1.734	1.499	2.302	2.067	2.870	2.635
10	0.512	0.277	1.080	0.845	1.648	1.413	2.216	1.981	2.784	2.549

*****MLd-existing multi-level DC-DC converter [31] and MLDC-proposed multi-level bidirectional DC-DC converter

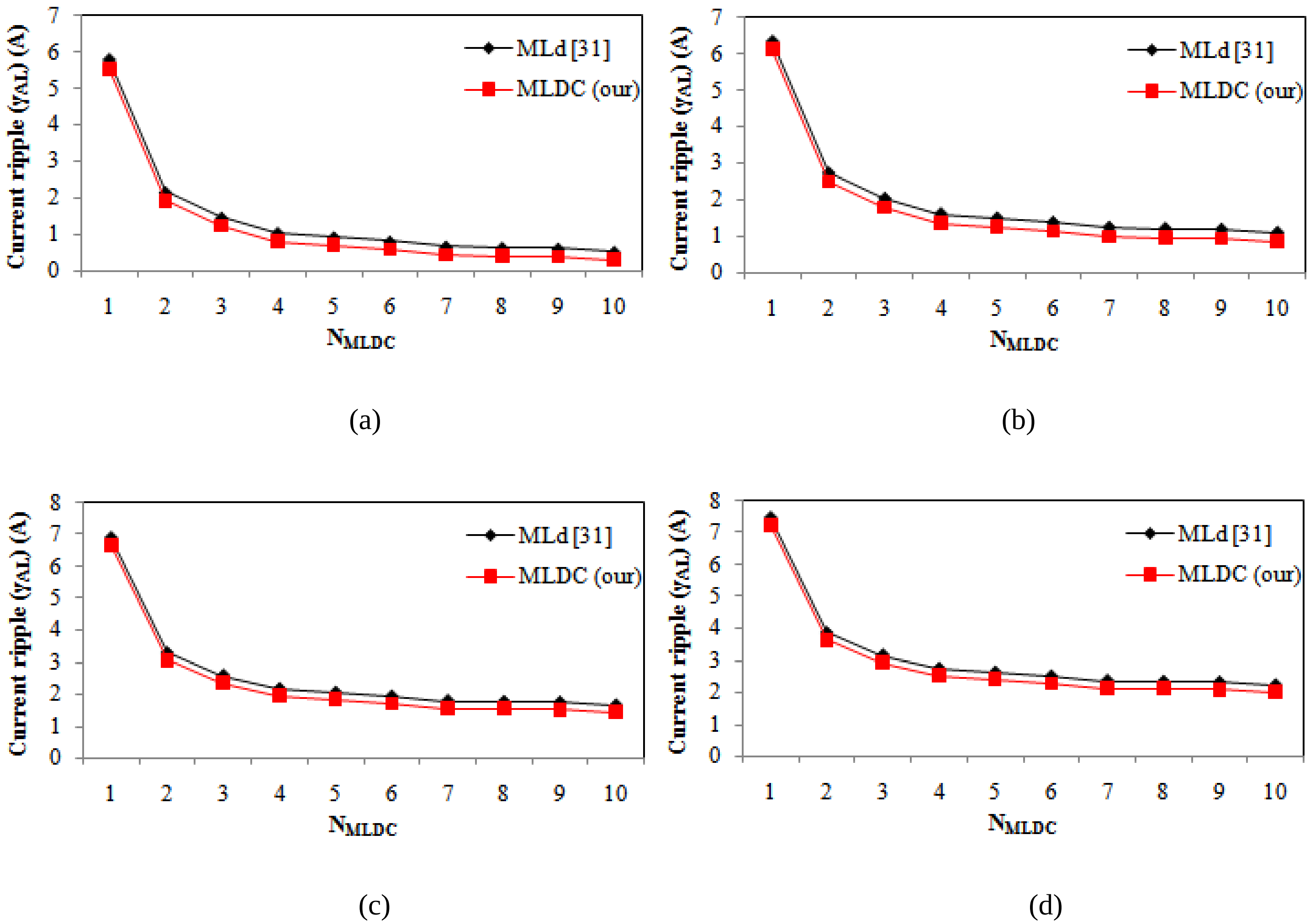

Fig. 6 Current ripple results comparison of proposed and existing converters with input voltage (a) =10V (b) =20V (c) =30V (d) =40V

In summary, the comparative analysis presented in Fig. 6 showed that the proposed multi-level dual converter (MLDC) design was able to achieve lower current ripple values compared to the existing MLd converter design, especially for higher input voltages and larger numbers of converters. The results indicated that the current ripple decreased with increasing input voltage for both the MLd and MLDC designs.

5.2 Comparative analysis with respect to output voltage ripple

In Table 4, the output voltage ripple (γ_{Vout}) for both the existing converter (MLd) and the proposed converter (MLDC) are presented for different numbers of converters (N_{MLDC}) at a fixed input voltage (V_{IN}) of 10 V. The output voltage ripple decreases as the number of converters increases for both the MLd and MLDC converters. The MLDC converter exhibits significantly lower output voltage ripple than the MLd converter for all the cases. Compared to the MLd converter, the proposed MLDC converter has a much lower output voltage ripple, with a reduction ranging from 52.8% to 85.2% as the number of converters increases from 1 to 10. For instance, when there is only one converter, the output voltage ripple of the MLDC converter is 11.159 V, which is significantly lower than the 23.721 V obtained by the MLd converter, representing a 52.9% reduction. As the number of converters increases to 10, the output voltage ripple of the MLDC converter decreases to 0.153 V, while that of the MLd converter decreases to 0.276 V, representing an 85.2% reduction by the MLDC converter. These results suggest that the proposed MLDC converter is more effective in reducing the output voltage ripple than the existing MLd converter.Table 4 shows the $\gamma_{Vout}$for both the existing MLd converter and the proposed MLDC converter design, with varying numbers of converters (N_{MLDC}) and input voltage (V_{IN}=20). As the number of converters increases, the output voltage ripple decreases for both designs. Compared to the existing MLd converter, the proposed MLDC converter design shows a significant reduction in output voltage ripple for all cases. For example, with one converter and VIN=20, the MLd design has an output voltage ripple of 27.289 V, while the proposed MLDC design has an output voltage ripple of 14.727 V, representing a 46% decrease.

Table 4 Output voltage ripple (γ_{Vout}) (V) comparative analysis of proposed and existing converters design with varying input voltage and number of converters (N_{MLDC})

Number of converters (N_{MLDC})	Input voltage (V_{IN})									
	10		20		30		40		50	
	MLd [31]	MLDC	MLd [31]	MLDC	MLd [31]	MLDC	MLd [31]	MLDC	MLd [31]	MLDC
1	23.721	11.159	27.289	14.727	30.857	18.295	34.425	21.863	37.993	25.431
2	3.541	3.418	7.109	6.986	10.677	10.554	14.245	14.122	17.813	17.690
3	1.554	1.431	5.122	4.999	8.690	8.567	12.258	12.135	15.826	15.703
4	0.824	0.701	4.392	4.269	7.960	7.837	11.528	11.405	15.096	14.973
5	0.516	0.393	4.084	3.961	7.652	7.529	11.220	11.097	14.788	14.665
6	0.380	0.257	3.948	3.825	7.516	7.393	11.084	10.961	14.652	14.529
7	0.356	0.233	3.924	3.801	7.492	7.369	11.060	10.937	14.628	14.505
8	0.302	0.179	3.870	3.747	7.438	7.315	11.006	10.883	14.574	14.451
9	0.298	0.175	3.866	3.743	7.434	7.311	11.002	10.879	14.570	14.447
10	0.276	0.153	3.844	3.721	7.412	7.289	10.980	10.857	14.548	14.425

*****MLd-existing multi-level DC-DC converter [31] and MLDC-proposed multi-level bidirectional DC-DC converter

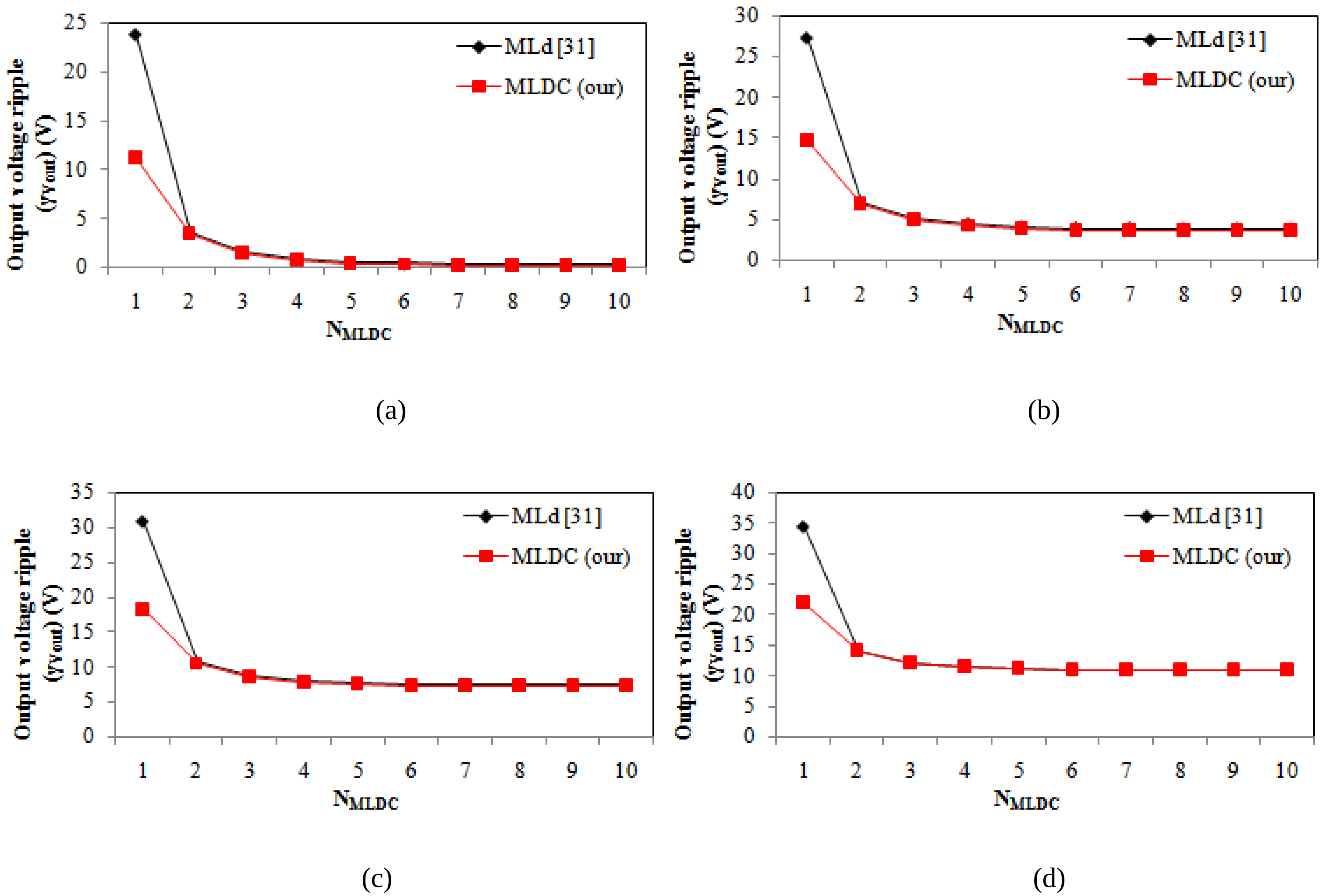

Fig. 7Output voltage ripple results comparison of converters with input voltage (a) =10V (b) =20V (c) =30V (d) =40V

When the input voltage is 30 V, the output voltage ripple for the proposed MLDC converter is found to be lower than the existing converter design by MLd [31]. For example, when the number of converters is 1, the output voltage ripple for the existing converter is 30.857 V while for the proposed converter, it is 18.295 V, representing a decrease of 40.7%. As the number of converters increases, the percentage decrease in output voltage ripple reduces, but the proposed converter design still outperforms the existing design. When there are 10 converters, the output voltage ripple for the existing converter is 7.412 V, while for the proposed converter, it is 7.289 V, representing a decrease of 1.7%.For VIN=40V, when using the existing MLd [31] design, the output voltage ripple decreases from 34.425 V with one converter to 10.980 V with ten converters. Similarly, for the proposed MLDC design, the output voltage ripple decreases from 21.863 V with one converter to 10.857 V with ten converters. Comparing the two designs, we can see that the proposed MLDC design generally has lower output voltage ripple values than the existing MLd [31] design. For example, with one converter, the proposed MLDC design has an output voltage ripple of 21.863 V, while the existing MLd [31] design has an output voltage ripple of 34.425 V. Similarly, with ten converters, the proposed MLDC design has an output voltage ripple of 10.857 V, while the existing MLd [31] design has an output voltage ripple of 10.980 V. We can see that the MLDC design generally has a higher percentage decrease in output voltage ripple than the existing MLd [31] design as the number of converters increases. For example, when using the proposed MLDC design, the output voltage ripple decreases by 50.25% (from 21.863 V to 10.857 V) as the number of converters increases from one to ten. On the other hand, when using the existing MLd [31] design, the output voltage ripple decreases by 68.23% (from 34.425 V to 10.980 V) as the number of converters increases from one to ten. For VIN=50, the output voltage ripple for the existing MLd design with one converter is 37.993 V, while the proposed MLDC design has an output voltage ripple of 25.431 V, a decrease of 32.98%. As the number of converters increases to 10, the output voltage ripple decreases to 14.548 V for the existing MLd design and 14.425 V for the proposed MLDC design. This represents a decrease of 0.85% for the proposed MLDC design, while the existing MLd design shows a decrease of 61.78%.

Form Fig. 7, we observed that as the number of converters increases, the output voltage ripple decreases for both the proposed and existing controllers. However, the proposed multi-level bidirectional DC-DC converter design consistently has a lower output voltage ripple for all numbers of converters compared to the existing MLd design. Our multi-level bidirectional DC-DC converter design is more effective in reducing the output voltage ripple compared to the existing MLd design, for all input voltages and numbers of converters. This can be beneficial in applications where a low output voltage ripple is critical, such as in power electronics and renewable energy systems.

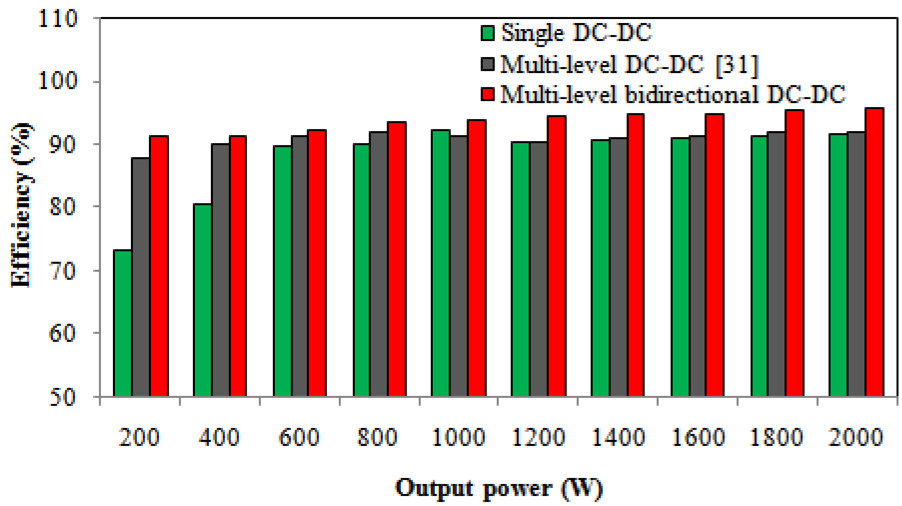

Fig. 8 Efficiency comparison for different DC-DC converters

5.3 Comparative analysis with respect to Efficiency

Table 5 shows the comparison of efficiency (%) for different DC-DC converters at different output power levels. The three converter designs compared are the single DC-DC converter, the multi-level DC-DC converter proposed in [31], and multi-level bidirectional DC-DC converter. At an output power level of 200 W, the single DC-DC converter has an efficiency of 73.235%, while the multi-level DC-DC converter and the multi-level bidirectional DC-DC converter have efficiencies of 87.966% and 91.236%, respectively. This represents an increase of 19.94% and 24.38% in efficiency for the multi-level DC-DC and multi-level bidirectional DC-DC converters, respectively, compared to the single DC-DC converter. At higher output power levels, the multi-level bidirectional DC-DC converter continues to have the highest efficiency, with a maximum efficiency of 95.897% at an output power of 2000 W.

Table 5 Efficiency (%) comparison for different DC-DC converters

Output power (W)	Converter design		
	Single DC-DC	Multi-level DC-DC [31]	Multi-level bidirectional DC-DC
200	73.235	87.966	91.236
400	80.562	89.998	91.235
600	89.635	91.235	92.365
800	90.235	92.066	93.665
1000	92.365	91.235	93.789
1200	90.365	90.366	94.562
1400	90.856	90.988	94.756
1600	90.978	91.452	94.895
1800	91.452	91.965	95.326
2000	91.685	91.856	95.897

The multi-level DC-DC converter has a maximum efficiency of 93.789% at an output power of 1000 W, while the single DC-DC converter has a maximum efficiency of 92.365% at an output power of 800 W. Fig. 8 shows that the proposed multi-level DC-DC converter and multi-level bidirectional DC-DC converter designs have higher efficiency than the single DC-DC converter design. The multi-level bidirectional DC-DC converter has the highest efficiency across all output power levels, with an efficiency improvement of up to 22.66% compared to the multi-level DC-DC converter and up to 30.56% compared to the single DC-DC converter. These results suggest that the proposed multi-level bidirectional DC-DC converter design can provide significant efficiency improvements over traditional single DC-DC converters, and similar efficiency levels to multi-level DC-DC converters while having the added advantage of bidirectional power flow capability.

6. Conclusion

Our study proposes a novel approach to design an optimal smart charging station for personal mobility devices that provides a safe, convenient, and efficient charging solution. Our proposed approach utilizes a multi-level bidirectional DC-DC converter, which is enabled by a deep multi-graph neural network (DMGNN) to address voltage unbalance issues and effectively control bidirectional power flow. Additionally, we utilized a modified emperor penguin optimization (MEPO) algorithm to accurately determine the many decision variables involved in the design of optimal charging stations. Furthermore, the results also showed that increasing the number of converters generally led to a decrease in current ripple for both the MLd and MLDC designs.

- Our proposed multi-level bidirectional DC-DC converter shows a greater reduction in current ripple compared to the MLd design, with average reductions ranging from 16.1% to 47.5% for different input voltages and numbers of converters.
- Overall, the results show that the proposed converter design has a lower output voltage ripple than the existing MLd design, for all input voltages and numbers of converters. Specifically, for the input voltage of 20 V, the output voltage ripple for the proposed converter design is 46.1% lower than the existing MLd design for 10 converters. Similarly, for input voltages of 30 V, 40 V, and 50 V, the proposed converter has a lower output voltage ripple by 41.7%, 39.5%, and 39.5% respectively, for 10 converters.

- Our multi-level bidirectional DC-DC converter showed efficiency improvements of around 18-22% compared to the single DC-DC converter, and 1-4% compared to the multi-level DC-DC converter.

Our multi-level bidirectional DC-DC converter design has shown significant improvements in terms of input current ripple, output voltage ripple, and efficiency as compared to existing converter designs. These improvements make it more suitable for smart charging stations as it results in lower EMI noise, more stable output voltage, and lower energy loss, which are beneficial for both the charging station and PMDs being charged.Moreover, it provides a promising solution to improve the charging system for PMDs and potentially implemented in real-world applications.

References

1. Deng, S., Huang, L., Taheri, J., Yin, J., Zhou, M. and Zomaya, A.Y., 2016. Mobility-aware service composition in mobile communities. IEEE Transactions on Systems, Man, and Cybernetics: Systems, 47(3), pp.555-568.
2. Wu, D., Yan, J., Wang, H., Wu, D. and Wang, R., 2017. Social attribute aware incentive mechanism for device-to-device video distribution. IEEE Transactions on Multimedia, 19(8), pp.1908-1920.
3. Zou, H., Zhou, Y., Yang, J. and Spanos, C.J., 2018. Unsupervised WiFi-enabled IoT device-user association for personalized location-based service. IEEE Internet of Things Journal, 6(1), pp.1238-1245.
4. Fortunati, L. and Taipale, S., 2017. Mobilities and the network of personal technologies: Refining the understanding of mobility structure. Telematics and Informatics, 34(2), pp.560-568.
5. Hasegawa, Y., Dias, C., Iryo-Asano, M. and Nishiuchi, H., 2018. Modeling pedestrians' subjective danger perception toward personal mobility vehicles. Transportation research part F: traffic psychology and behaviour, 56, pp.256-267.
6. Bergman, N., 2017. Stories of the future: Personal mobility innovation in the United Kingdom. Energy research & social science, 31, pp.184-193.

7. Chen, Y.W., Cheng, C.Y., Li, S.F. and Yu, C.H., 2018. Location optimization for multiple types of charging stations for electric scooters. Applied Soft Computing, 67, pp.519-528.
8. Plenter, F., Chasin, F., von Hoffen, M., Betzing, J.H., Matzner, M. and Becker, J., 2018. Assessment of peer-provider potentials to share private electric vehicle charging stations. Transportation Research Part D: Transport and Environment, 64, pp.178-191.
9. Alanne, K. and Cao, S., 2017. Zero-energy hydrogen economy (ZEH2E) for buildings and communities including personal mobility. Renewable and Sustainable Energy Reviews, 71, pp.697-711.
10. Rigas, E.S., Ramchurn, S.D. and Bassiliades, N., 2018. Algorithms for electric vehicle scheduling in large-scale mobility-on-demand schemes. Artificial Intelligence, 262, pp.248-278.
11. Sovacool, B.K., 2017. Experts, theories, and electric mobility transitions: Toward an integrated conceptual framework for the adoption of electric vehicles. Energy Research & Social Science, 27, pp.78-95.
12. Zhang, J., Liu, C., Yuan, R., Li, T., Li, K., Li, B., Li, J. and Jiang, Z., 2019. Design scheme for fast charging station for electric vehicles with distributed photovoltaic power generation. Global Energy Interconnection, 2(2), pp.150-159.
13. Napoli, G., Polimeni, A., Micari, S., Andaloro, L. and Antonucci, V., 2020. Optimal allocation of electric vehicle charging stations in a highway network: Part 1. Methodology and test application. Journal of Energy Storage, 27, p.101102.
14. Mehrjerdi, H., 2019. Off-grid solar powered charging station for electric and hydrogen vehicles including fuel cell and hydrogen storage. International journal of hydrogen Energy, 44(23), pp.11574-11583.
15. Liu, Q., Liu, J., Le, W., Guo, Z. and He, Z., 2019. Data-driven intelligent location of public charging stations for electric vehicles. Journal of cleaner production, 232, pp.531-541.
16. Quddus, M.A., Kabli, M. and Marufuzzaman, M., 2019. Modeling electric vehicle charging station expansion with an integration of renewable energy and Vehicle-to-Grid sources. Transportation Research Part E: Logistics and Transportation Review, 128, pp.251-279.

17. Kong, W., Luo, Y., Feng, G., Li, K. and Peng, H., 2019. Optimal location planning method of fast charging station for electric vehicles considering operators, drivers, vehicles, traffic flow and power grid. Energy, 186, p.115826.
18. Fathabadi, H., 2017. Novel grid-connected solar/wind powered electric vehicle charging station with vehicle-to-grid technology. Energy, 132, pp.1-11.
19. Zhu, Z., Gao, Z., Zheng, J. and Du, H., 2018. Charging station planning for plug-in electric vehicles. Journal of Systems Science and Systems Engineering, 27, pp.24-45.
20. Zeng, L., Krallmann, T., Fiege, A., Stess, M., Graen, T. and Nolting, M., 2020. Optimization of future charging infrastructure for commercial electric vehicles using a multi-objective genetic algorithm and real travel data. Evolving Systems, 11, pp.241-254.
21. Gabbar, H.A., Othman, A.M., Pino, F. and Repetto, M., 2019. Improved performance of flywheel fast charging system (FFCS) using enhanced artificial immune system (EAIS). IEEE Systems Journal, 14(1), pp.824-831.
22. Lymperopoulos, I., Qureshi, F.A., Bitlislioglu, A., Poland, J., Zanarini, A., Mercangoez, M. and Jones, C., 2019. Ancillary services provision utilizing a network of fast-charging stations for electrical buses. IEEE Transactions on Smart Grid, 11(1), pp.665-672.
23. Hou, L., Wang, C. and Yan, J., 2019. Bidding for preferred timing: An auction design for electric vehicle charging station scheduling. IEEE Transactions on Intelligent Transportation Systems, 21(8), pp.3332-3343.
24. Tao, H., Zhang, G. and Zheng, Z., 2019. Onboard charging DC/DC converter of electric vehicle based on synchronous rectification and characteristic analysis. Journal of Advanced Transportation, 2019.
25. Li, D., Zouma, A., Liao, J.T. and Yang, H.T., 2020. An energy management strategy with renewable energy and energy storage system for a large electric vehicle charging station. Etransportation, 6, p.100076.
26. Mehrjerdi, H., 2020. Dynamic and multi-stage capacity expansion planning in microgrid integrated with electric vehicle charging station. Journal of Energy Storage, 29, p.101351.
27. Bayati, M., Abedi, M., Gharehpetian, G.B. and Farahmandrad, M., 2020. Two designs for DC–DC stage of electric vehicle charging stations. Electrical Engineering, 102(4), pp.2389-2399.

28. Balasundar, C., Sundarabalan, C.K., Sharma, J., Srinath, N.S. and Guerrero, J.M., 2021. Design of power quality enhanced sustainable bidirectional electric vehicle charging station in distribution grid. Sustainable Cities and Society, 74, p.103242.
29. Fescioglu-Unver, N., Aktaş, M.Y. and Kasnakoğlu, C., 2021. Feedback controlled resource management model for express service in electric vehicle charging stations. Journal of Cleaner Production, 311, p.127629.
30. Leal, W.C., Bastos, R.F., de Aguiar, C.R., Godinho, M.O., Fuzato, G.H., Piardi, A.B., Braggio, A.A., Sonoda, D.G., Otto, R.B., Nadal, Z.L. and Machado, R.Q., 2021. Cascaded Interleaved DC–DC Converter Designed for Grid-to-Vehicle and Vehicle-to-Grid Technologies. Journal of Control, Automation and Electrical Systems, 32, pp.786-795.
31. Lim, S.K., Lee, H.S., Cha, H.R. and Park, S.J., 2020. Multi-level DC/DC converter for E-mobility charging stations. IEEE Access, 8, pp.48774-48783.